Inorganic Chemistry
Article
pubs.acs.org/IC

Hydration Properties of the Zn^{2+} Ion in Water at High Pressure

Valentina Migliorati,*[,†] Giordano Mancini,[‡,§] Simone Tatoli,[†] Andrea Zitolo,[†] Adriano Filipponi,[‖] Simone De Panfilis,[⊥] Andrea Di Cicco,[⊗] and Paola D'Angelo*[,†]

[†]Dipartimento di Chimica, Università di Roma "La Sapienza", P.le Aldo Moro 5, 00185 Roma, Italy
[‡]CASPUR, Inter-University Consortium for Supercomputing in Research, via dei Tizii 6b, 00185 Roma, Italy
[§]Scuola Normale Superiore, Classe di Scienze, Pisa, Italy
[‖]Dipartimento di Scienze Fisiche e Chimiche, Università degli Studi dell'Aquila, Via Vetoio, 67100 L'Aquila, Italy
[⊥]Centre for Life Nano Science - IIT@Sapienza, Dipartimento di Fisica, Università di Roma "La Sapienza", P.le Aldo Moro 2, 00185 Roma, Italy
[⊗]CNISM, Sezione di Fisica, Scuola di Scienze e Tecnologie, Università di Camerino, 62032 Camerino (MC), Italy

Supporting Information

ABSTRACT: The structure and dynamics of water in ionic solutions at high pressure have been investigated using a combined approach based on extended X-ray absorption fine structure (EXAFS) spectroscopy and Molecular Dynamics (MD) simulations. Modification of the hydration properties of the Zn^{2+} ion induced by a pressure increase from ambient condition up to ~6.4 GPa has been revealed and accurately analyzed. With increasing pressure the first hydration shell of the Zn^{2+} ion has been found to retain an octahedral symmetry with a shortening of the Zn−O distance up to 0.09 Å and an increased width associated with thermal motion, as compared to the ambient condition hydration complex. A very interesting picture of the dynamic behavior of the first hydration shell has emerged from the analysis of the simulations: up to 2.5 GPa no exchange events between first and second shell water molecules occurred, while above this pressure value several exchange events take place in the solution following an associative interchange mechanism. This result can be explained by the very high compression and packing of the solvent which force second shell water molecules to enter the Zn^{2+} first hydration shell. MD simulations indicate a strong pressure effect also on the structure of the second coordination shell which is compressed and becomes more disordered and less structured with increasing pressure. The water mobility and the ion diffusion coefficient have been found to increase in the high density conditions, as a consequence of the rupture of the hydrogen bond network caused by pressure.

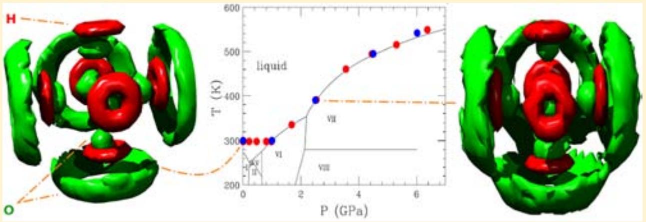

1. INTRODUCTION

The properties of aqueous solutions under pressure are of fundamental importance for a wide range of scientific disciplines, such as geoscience, environmental sciences, and planetary modeling. They are essential for instance to understand the physicochemical properties of water and salt solutions in the Earth mantle[1,2] and icy satellites,[3] as well as to comprehend the effect of pressure on chemical processes.[4] At high temperatures and pressures water exists in different liquid or solid phases whose properties are very different from those found at ambient conditions. Supercritical water exists at temperatures above 600 K and pressures between 10 MPa and 1 GPa. It is characterized by a low dielectric constant (~6 in a typical supercritical regime) and weak hydrogen bonding formation which makes it an excellent solvent for non polar substances. Because of the broad range of applications, such as in the decomposition of organic wastes or in the hydrothermal synthesis, supercritical water has been extensively studied.[5−7] At pressures between 0.1 and 10 GPa and temperatures between 300 and 500 K the complexity of water interactions results in a rich polymorphic phase diagram with several high density ice crystal structures and a compressed liquid water phase above the melting line. The increased interest in the properties of water at high-pressure stimulated the development of specific experimental techniques. The effect of pressure on the structure and hydrogen bond network of compressed water has been recently addressed by a variety of experimental and theoretical works.[8−14] Although different conclusions are drawn from these studies, they suggest the possible existence of a high-density state of water (HDW) which at a pressure of few kilobars gradually evolves at the expense of a low-density state of water (LDW).[11,15,16] In HDW the second shell of neighbor molecules is thought to collapse onto the first one, as a consequence of the rupture of the hydrogen bond network. Despite the plethora of studies on the properties of pure high-density water, there are only few works in the literature addressing the structural changes of ionic aqueous solutions under high

Received: November 19, 2012
Published: December 31, 2012

dx.doi.org/10.1021/ic302530k | *Inorg. Chem.* 2013, 52, 1141−1150

pressure.[17−19] In one study the transformation of the Rb^+ and Br^- first hydration shells was investigated by means of X-ray absorption spectroscopy (XAS), and dramatic effects in the anion hydration structure have been observed with increasing pressure.[17]

Here, we present an extensive study of the hydration properties of the Zn^{2+} ion in conditions of very high pressures (up to ∼6.4 GPa), combining extended X-ray absorption fine structure (EXAFS) and Molecular Dynamics (MD) simulations. Zn^{2+} is well-known to form in water a first shell complex consisting of six tightly bound solvent molecules arranged in an octahedral symmetry.[20−30] The powerful approach which combines XAS and MD simulations has been previously applied by our group to the study of several cations and anions in aqueous and non aqueous solvents at ambient conditions.[31−45] Here, this integrated procedure is used to investigate the pressure effects on the hydration structure of the Zn^{2+} ion, as well as on the dynamic properties of the water molecules surrounding the ion.

2. METHODS

2.1. X-ray Absorption Measurements and Data Analysis. Zn K-edge X-ray absorption spectra (XAS) were collected at the BM29 beamline[46] of the European Synchrotron Radiation Facility using the large-volume high-pressure setup based on the Paris-Edinburgh press. The storage ring was operating in uniform mode with typical currents in the 200−160 mA range between refills. The bending magnet source was monochromatized with a Si(311) energy scanning double crystal monochromator and vertically focalized to about 50 μm using a Rh coated bent mirror at 3.5 mrad incidence for harmonic rejection.[47] The horizontal beam size was set by secondary slits to 0.8 mm to probe the central part of the sample container.

The sample was a 0.5 M Zn^{2+} aqueous solution obtained by dissolving the appropriate amount of $Zn(NO_3)_2$ in water. The nitrate counterion has been chosen to prevent the formation of ionic pairs in the solution. The sample was confined in a Teflon cylindrical container with a 1.1 mm internal cylindrical cavity inserted in a doubly conical 7 mm boron-epoxy gasket as illustrated in Figure 1. Heating (when required) was obtained passing a suitable current through the cylindrical graphite resistor surrounding the sample container using electrical cables connected with the upper and lower WC anvils while squeezing the sample at the required pressure. The sample concentration was optimized for the collection of high quality transmission spectra (but still sufficiently low to guarantee a fully hydrated specimen) and, owing to the high absorption of the gasket material, the high beam intensity and spectral purity achievable with the mirror setup were also essential for this purpose. Ancillary techniques such as sample temperature scanning capabilities[48] and a MAR area detector for the collection of X-ray Diffraction (XRD) from the crystalline sample powder components were also available and used for sample check and calibration purposes.

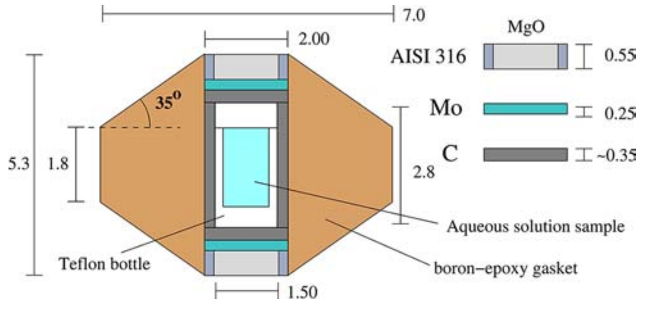

Figure 1. Schematic drawing of the (cylindrically symmetric) sample section showing boron-epoxy gasket, graphite heater (C), Teflon bottle, and its internal cavity filled with the $Zn(NO_3)_2$ aqueous solution. The dimensions in mm refer to the parts as assembled prior to pressurization.

The sample history on the (P,T) diagram is illustrated in Figure 2: the red circles represent the thermodynamic equilibrium parameters where XAS spectra were collected. The sample was first progressively pressurized at room temperature T_a = 296 K, and a few data points were collected in the equilibrium liquid phase until the liquid water-ice VI line was crossed. For higher pressures the sample was also heated following the water melting line. High quality spectra were collected up to ∼6.4 GPa and 550 K, a safe limit prior to the complete closure of the gap between the anvils. After heater switch-off and pressure release to ambient conditions a final XAS measurement was collected to check sample integrity and absence of chemical reactions between sample and container components, retrieving the known Zn^{2+} aqueous solution spectrum at ambient condition.

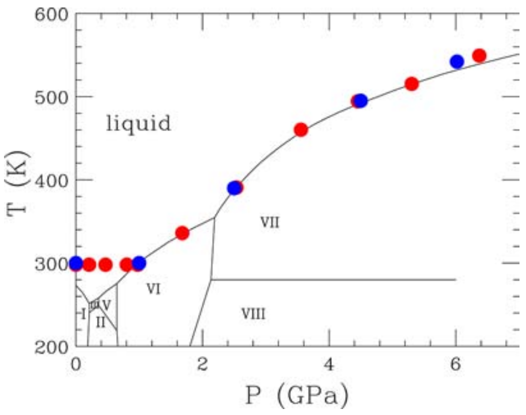

Figure 2. Thermodynamic parameters of the $Zn(NO_3)_2$ 0.5 M aqueous solution corresponding to the experimental XAS measurements (red filled circles) and to the MD simulations (blue filled circles). The phase diagram of pure water is reported for reference.

At pressures corresponding to the ice VI or ice VII stability regions the water salt mixture phase diagrams are not precisely known, but they are expected to be of eutectic type in the water reach region corresponding to the sample composition. For T below the eutectic temperature $T_e(P)$ the sample separates into the stable ice phase and a minority component of hydrated salt phase. By raising the temperature at (and above) $T_e(P)$ the hydrated salt phase melts together with an appropriate fraction of ice and separates into a highly concentrated liquid phase with the Zn^{2+} concentration corresponding to the liquidus line and a residual ice. By further raising the temperature the molten fraction increases. The sample is fully melted when T reaches the liquidus line, that, for low concentrations, corresponds to a temperature close to the ice melting temperature $T_m(P)$. Evidence for high pressure sample crystallization is directly obtained from the XRD area detector but also from the XAS data. At a given P and intermediate $T_e(P) < T < T_m(P)$ Zn^{2+} ions are surrounded by molten water so X-ray absorption may result in a misleading probe of the sample state. In this temperature range, however, the sample shows a mechanical instability (due to gravity effect on the two phases with different densities) which results in a time dependent absorption level. While the presence of ice can be directly confirmed by XRD a very convenient diagnostic probe is obtained by monitoring the X-ray absorption above the Zn K-edge during controlled temperature scans.[49] The scans are useful to mark both $T_e(P)$ and $T_m(P)$ and to bring the sample at the desired thermodynamic state on the melting line.

In this experiment the thermodynamic sample state parameters (P,T) were estimated from the oil pressure and supplied heating electric power (which is proportional to the temperature difference from T_a in this relatively narrow T range), using well established calibration curves obtained in many previous equivalent experiments with a similar heater/gasket geometry. We did not put a thermocouple into the heated sample region to avoid the risk to produce a leak in the container. The reliability of these estimates was checked by the correct prediction of the melting line crossing and from the angular aperture of some ice VI or ice VII Debye−Scherrer rings revealed at T_a by the XRD area detector. The resulting uncertainty of the corresponding (P,T) values along the melting line is estimated to be around 8%.

The Extended X-ray Absorption Fine Structure (EXAFS) analysis has been carried out by means of the GNXAS program, and a thorough description of the theoretical framework can be found in ref 50. A detailed EXAFS investigation was previously carried out on a 0.2 M $Zn(NO_3)_2$ aqueous solution at standard conditions.[21] The EXAFS data analysis showed the existence of an octahedral hydration shell with 6 oxygen atoms at 2.078(2) Å and 12 hydrogen atoms at 2.78(2) Å, while the second hydration shell was found to provide a negligible contribution to the experimental spectrum. In the present work the EXAFS data analysis has been carried out on the basis of these results including both the Zn−O and the Zn−H first shell contributions. These shells have been modeled with gamma-like distribution curves with mean distance R, standard deviation σ, and skewness β that can be varied in a wide range in a continuous manner. In addition, the multiple scattering (MS) signals associated with the 3 linear and 12 rectangular O−Zn−O configurations within the first hydration shell have been included in the theoretical calculations. Phase shifts, $A(k,r)$ and $\phi(k,r)$, have been calculated starting from one of the MD configurations, by using muffin-tin potentials and advanced models for the exchange-correlation self-energy (Hedin−Lundqvist). The values of the muffin-tin radii are 0.2, 0.9, and 1.2 Å, for hydrogen, oxygen, and zinc, respectively. Inelastic losses of the photoelectron in the final state have been accounted for intrinsically by a complex potential. The imaginary part also includes a constant factor accounting for the core-hole width (1.67 eV). Two nonstructural parameters were minimized, namely, E_0 (core ionization threshold) and S_0^2 (many body amplitude reduction factor). The quality of the fits was determined by the goodness-of-the-fit parameter.[51,50]

2.2. Molecular Dynamics Simulations.

Molecular Dynamics (MD) simulations of the Zn^{2+} ion in aqueous solution have been performed using an effective two-body potential obtained by fitting the parameters of a suitable analytical function on an ab initio potential energy surface (PES) as described in ref 23. The ab initio PES was generated taking into account scalar relativistic effects using a suitable effective core potential and including many-body effects by means of the polarizable continuum model (PCM).[52] A thorough description of the procedure used to obtain the ab initio potential energy function can be found in ref 23. As far as the water−water interactions are concerned, the SPC/E water model has been employed,[53] since it provides a very good description of the structural and dynamic properties of liquid water at ambient conditions.[54] Moreover, the SPC/E model was shown to accurately predict the thermodynamic properties of water also at high pressures and temperatures.[55] The Zn^{2+}-water two-body potential has the following analytical function:

$$V(r) = \frac{q_i q_o}{r_{io}} + \frac{A_o}{r_{io}^4} + \frac{B_o}{r_{io}^6} + \frac{C_o}{r_{io}^8} + \frac{D_o}{r_{io}^{12}} + E_o e^{-F_o r_{io}} + \sum_{ih=ih1,ih2} \frac{q_i q_h}{r_{ih}} + \frac{A_h}{r_{ih}^4} + \frac{B_h}{r_{ih}^6} + \frac{C_h}{r_{ih}^8} + \frac{D_h}{r_{ih}^{12}} \quad (1)$$

where r_{io}, r_{ih1}, and r_{ih2} are the ion−water distances; q_i q_o, and q_h are the electrostatic charges of Zn^{2+}, oxygen, and hydrogen in the SPC/E water model, respectively (2.0, −0.8476, and 0.4238 au). A_0, ..., F_0 and A_h, ..., D_h are the parameters obtained by the fitting procedure (see ref 23). Five simulations of Zn^{2+} in aqueous solution were carried out to reproduce the properties of the system in five different points of the phase diagram, that is, 300 K and 0.1 MPa (ρ = 1006.8 g/L), 300 K and 1.0 GPa (ρ = 1271.2 g/L), 390 K and 2.5 GPa (ρ = 1358.8 g/L), 495 K and 4.5 GPa (ρ = 1458.9 g/L), and 542 K and 6.02 GPa (ρ = 1523.2 g/L). The points of the water phase diagram investigated by means of MD simulations are shown in Figure 2. The density values used are those of pure water under high pressure and have been obtained by means of a modified version of the *Steam tables* code.[56] The points of the phase diagram investigated theoretically correspond to the experimental points up to 4.5 GPa, while the last point is slightly lower than the experimental one as it coincides with the highest pressure value for which it is possible to calculate the density of pure water at the chosen temperature using the *Steam tables* code.[56] Different box volumes have been employed to reproduce the chosen density, temperature, and pressure conditions. In particular, the box sides used are 29.0 Å, 27.1 Å, 26.3 Å, 25.6 Å, and 25.3 Å for the simulations at 0.1 MPa, 1 GPa, 2.5 GPa, 4.5 and 6.02 GPa respectively.

The simulations were carried out using the GROMACS package version 3.2.1,[57] modified to include the ion−water effective pair potentials. The system was composed by one Zn^{2+} ion and 819 water molecules (for a total of 2458 atoms) in a cubic box, using periodic boundary conditions. A cutoff of 9 Å was used to deal with non bonded interactions, with the Particle Mesh Ewald (PME) method to treat long-range electrostatic effects.[58] A homogeneous background charge has been used to compensate for the presence of the Zn^{2+} ion. The temperature was kept constant at the desired value using the Berendsen thermostat[59] with a coupling constant of 0.1 ps. A time step of 1 fs was employed, saving a configuration every 25 time steps and equilibrating the system for 5 ns before sampling. The production runs were 10 ns long.

2.3. Structural and Dynamic Analysis.

The structural properties of the Zn^{2+} aqueous solutions were described in terms of radial distribution functions, $g_{Zn-O}(r)$ and $g_{Zn-H}(r)$:

$$g_{AB}(r) = \frac{\langle \rho_B(r) \rangle}{\langle \rho_B \rangle_{local}} = \frac{1}{N_A \langle \rho_B \rangle_{local}} \sum_{i \in A}^{N_A} \sum_{i \in B}^{N_B} \frac{\delta(r_{ij} - r)}{4\pi r^2} \quad (2)$$

where $\langle \rho_B(r) \rangle$ is the particle density of type B at distance r around type A, and $\langle \rho_B \rangle_{local}$ is the particle density of type B averaged over all spheres around particle A with radius r_{max} (half the box length).

Angular distribution functions (a.d.f.) have been calculated for three different angles: the angle formed by two different Zn−O vectors in the first shell (labeled as ψ), the angle formed by the water dipole vector and the Zn−O vector direction (labeled as ϕ), and the angle formed by the normal to the water plane and the Zn−O vector direction (labeled as ζ).

To describe the distribution of water molecules around the Zn^{2+} ion, spatial distribution functions were also calculated.

The mean residence time of water molecules in the Zn^{2+} first hydration shell has been evaluated using the approach called the "direct method" proposed by Hofer et al.[60] This method scans the whole trajectory for movements of the ligands, either entering or leaving the first coordination shell. Whenever a ligand crosses the boundaries of the shell, its further path is followed, and if its new placement outside or inside the shell lasts for more than a chosen t^*, the event is accounted for as a "real" exchange process. The water residence τ_d is then calculated as

$$\tau_d = \frac{t_{sim} \overline{n}}{N_{ex}} \quad (3)$$

where t_{sim} is the total simulation time, $\overline{n}$ is the average first shell coordination number, and N_{ex} is the number of "real" solvent exchanges between the first hydration shell and the rest of the solvent.

The Zn^{2+} diffusion coefficient, D_{Zn}, has been determined from the mean square displacement (MSD) using the Einstein relation

$$D_{Zn} = \frac{1}{6} \lim_{t \to \infty} \frac{\langle \| \mathbf{r}_{Zn}(t) - \mathbf{r}_{Zn}(0) \|^2 \rangle}{t} \quad (4)$$

where $\mathbf{r}_{Zn}(0)$ is the Zn^{2+} initial position and $\mathbf{r}_{Zn}(t)$ is the position of the ion at time t.

A detailed view of the dynamics of the water molecules surrounding the ion has been obtained using reorientational correlation functions, defined as[61]

$$C_l^{\alpha}(t) = \langle P_l(\mathbf{u}^{\alpha}(t) \cdot \mathbf{u}^{\alpha}(0)) \rangle \quad (5)$$

where P_l is the l-th rank Legendre polynomial, and $\mathbf{u}^{\alpha}(t)$ is a unit vector in a certain direction α at time t. By fitting $C_l(t)$ to an exponential function $C_l(t) = e^{-(t/\tau_l)}$, it is possible to determine the correlation time τ_l, defined as the rotation time of the $\mathbf{u}^{\alpha}$ vector. For our analyses we used $l = 1$ and three different vectors: the normal to the water molecular plane passing through the center of the oxygen atom $\mathbf{u}^N$, a vector along the HH direction $\mathbf{u}^{HH}$, and the water dipole vector $\mathbf{u}^D$; $\mathbf{u}^D$ is correlated to the dielectric relaxation rates while $\mathbf{u}^{HH}$ to ^{1}H-^{1}H NMR dipolar relaxation experiments.[62] Using an approach already implemented for pure water,[61] we have employed a mixed integration exponential fit method to evaluate the first rank correlation times, thus minimizing the noise introduced by the slow convergence of the correlation function tail. Direct integration was used in the initial part of the function, while the tail contribution was taken into account by means of an exponential fit. Because of the different behavior of first shell correlation functions caused by the presence of the ion, we have used different time windows for direct integration: a value of 15 ps was employed for $\mathbf{u}^D$, while the $\mathbf{u}^N$ and $\mathbf{u}^{HH}$ correlation functions were explicitly integrated up to 5 ps. As far as the correlation times of bulk water are concerned, the switch value was always 5 ps, the same as used in ref 61.

Standard GROMACS tools[57] have been used to calculate the reorientational correlation functions, diffusion coefficients, and spatial distribution functions (g_rotacf, g_msd, and g_sdf, respectively), while in-house written codes were employed for all of the other MD analyses.

3. RESULTS AND DISCUSSION

3.1. EXAFS Analysis of Zn^{2+} in High-Density Water.

The hydration structure of the Zn^{2+} ion in aqueous solution at ambient conditions is well-established. The first coordination sphere is composed of six water molecules arranged in an octahedral configuration with 6 Zn−O distances at 2.078(2) Å and 12 hydrogen atoms at 2.78(2) Å.[21] This coordination model has been used as the starting configuration for the analysis of all of the experimental EXAFS spectra collected at high pressure. In particular the EXAFS data analysis has been carried out including both the Zn−O and the Zn−H first shell two-body signals, and the MS signals associated with the linear and rectangular O−Zn−O configurations. Least-squares fits of the EXAFS spectra were performed in the range $k = 2.5−11.8$ Å^{-1} optimizing the whole set of structural and nonstructural parameters. In particular, we optimized four structural parameters for each single-shell contribution including the coordination numbers, and two additional structural parameters (the O−Zn−O angle and its variance) for the three-body contributions. The best-fit analysis of the ~6.4 GPa spectrum is shown in the upper panel of Figure 3, as an example. The first four curves from the top are the Zn−O and Zn−H first-shell $\gamma^{(2)}$ contributions, and the MS signals associated with the O−Zn−O linear and rectangular configurations. The remaining graphs of the figure show the comparison of the total theoretical contribution with the experimental spectrum. Overall, the fitted EXAFS spectrum matches the experimental data quite well and, as expected, the dominant contribution to the total EXAFS signals is given by the Zn−O first-shell signal, even though, because of the well-ordered structure of the water molecules around the ion, the 12 hydrogen atoms of the first hydration shell give rise to a rather strong $\gamma^{(2)}$ signal, which is detectable up to about $k = 8$ Å^{-1}. The contribution of the second hydration shell is negligible, while the MS paths from the O−Zn−O configurations yield detectable amplitude signals in the low-k regions of the spectra. The lower panel of Figure 3 shows the corresponding k^2-weighted Fourier transform (FT) calculated with no applied phase shift correction in the k range 2.5−11.8 Å^{-1}.

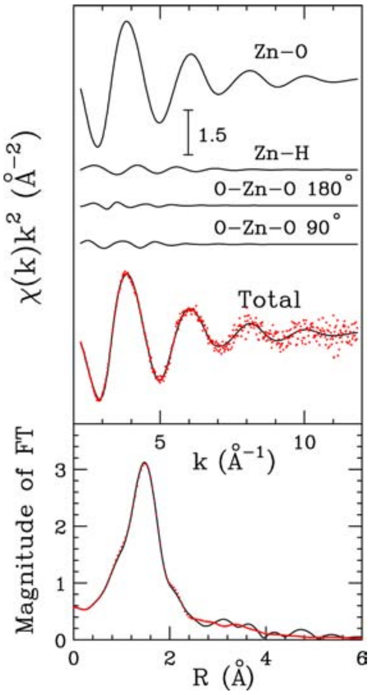

Figure 3. Fit of the ~6.4 GPa Zn^{2+} water solution EXAFS spectrum. From the top to the bottom the following curves are reported: the Zn−O first shell signal, the Zn−H first shell signal, the O−Zn−O linear and orthogonal three-body signals, the total theoretical signal (full black line) compared with the experimental spectrum (red dotted line). The lower panel shows the nonphase-shift-corrected Fourier transforms of the experimental data (red dotted line), and of the total theoretical signals (full black line).

Figure 4 shows the comparison between the EXAFS experimental data of the Zn^{2+} aqueous solutions collected at different pressure and temperature values (see red points in Figure 2) and the theoretical spectra obtained using the procedure described above. The high quality of the experimental data as well as the excellent agreement with the fitting model signal can be fully appreciated. The refined values

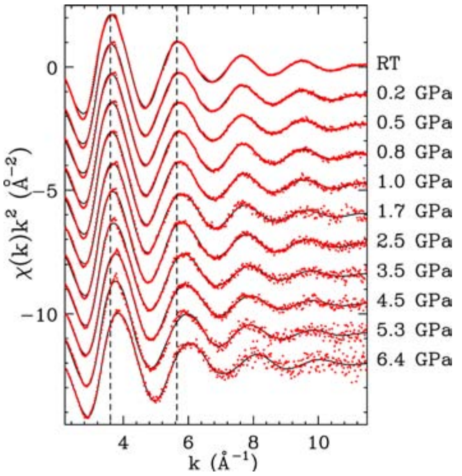

Figure 4. Comparison between the experimental (red dotted line) and the theoretical (black solid line) EXAFS signals for the Zn^{2+} aqueous solution at different pressure and temperature values (see Figure 2).

Table 1. Structural Parameters of Zn−O $g(r)$ First Peak Obtained from the EXAFS Analysis of the Zn^{2+} Aqueous Solutions at Different Pressure and Temperature Values (See Figure 2)[a]

	EXAFS				MD			
pressure	N	R(Å)	σ^2(Å^2)	β	N	R(Å)	σ^2(Å^2)	β
0.10 MPa	6.0(1)	2.078(2)	0.0087(5)	0.2(1)	6	2.076	0.0040	0.2
0.20 GPa	6.0(1)	2.065(5)	0.0087(5)	0.2(1)				
0.46 GPa	6.0(1)	2.063(5)	0.0089(5)	0.2(1)				
0.80 GPa	6.0(1)	2.062(5)	0.0090(5)	0.2(1)				
1.00 GPa	6.0(1)	2.058(5)	0.0090(5)	0.2(1)	6	2.066	0.0042	0.2
1.68 GPa	6.0(1)	2.048(5)	0.0095(5)	0.2(1)				
2.50 GPa	6.0(2)	2.044(6)	0.010(1)	0.2(1)	6	2.061	0.0053	0.2
3.55 GPa	6.0(2)	2.034(6)	0.011(1)	0.2(1)				
4.50 GPa	6.0(2)	2.018(7)	0.011(1)	0.2(1)	6	2.056	0.0064	0.2
5.30 GPa	6.0(3)	2.015(7)	0.011(1)	0.2(1)				
6.02 GPa					6	2.051	0.0069	0.2
6.37 GPa	6.0(3)	1.992(7)	0.011(1)	0.2(1)				

[a] N is the Zn−O coordination number, R is the mean Zn−O distance, σ is the Debye-Waller factor, and β is the asymmetry parameter. Errors are given in parentheses.

for the full set of structural parameters obtained from the minimization procedures are listed in Table 1. The frequencies of the EXAFS oscillations of Figure 4 reveal a structural trend with increasing pressure and temperature. In particular, a contraction of the first shell zinc-water distance occurs on going from ambient conditions to ~6.4 GPa, while only a very small decrease can be observed for the amplitude of the EXAFS signals. This finding is confirmed by the results of the analysis shown in Table 1. In particular, the Zn−O first shell distance undergoes a shortening of 0.09 Å in going from ambient condition to the highest measured pressure value, while no variation is observed for the number of first shell coordinated water molecules. Moreover, from the values of the angles associated with the MS paths (that have been found to be 180° and 90° for the linear and rectangular configurations in all fits) it is possible to asses that also the octahedral symmetry is retained for the Zn^{2+} hydration complexes.

The main result of the EXAFS analysis is that with increasing pressure there is a contraction of the average Zn−O bond length while the octahedral hydration shell is retained. To verify the reliability of this finding it is very important to establish whether in this case the EXAFS technique is able to determine the coordination numbers with sufficient accuracy. To this end a statistical analysis applying two-dimensional contour plots to selected parameters of the fit has been carried out to establish error limits in the refined parameters. This analysis examines the correlations among fitting parameters and evaluates the statistical errors by following the procedure described in detail in ref 51. Figure 5 shows the contour plots of the Zn−O coordination number and Debye−Waller (DW) factor for the ~6.4 GPa case, as an example, where the innermost contour refers to the 95% error confidence interval. Even if it is well-known that in the case of disordered systems there is a strong correlation between DW factors and coordination numbers as both parameters are related to the amplitude of the EXAFS oscillation, in this case the error associated with the first shell coordination number is quite small (0.3 for the ~6.4 GPa solution) proving the reliability of the obtained results. This is due to the high stability of the Zn^{2+} hydration complex that makes this species more similar to a molecular compound than to a fast exchanging hydration complex. This behavior is also reflected in the quite low values obtained for the DW factors and the rather small β values that testify the existence of an almost Gaussian distribution for the first shell peaks. The DW factor values tend to increase slightly with increasing pressure, and this explains the small reduction of amplitude observed in the EXAFS experimental signals. The Zn−O first shell distances determined from the EXAFS analysis for different pressure values show a linear decreasing trend upon compression (see Figure 6).

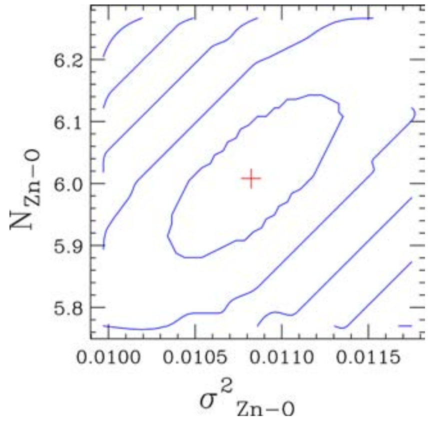

Figure 5. Two-dimensional contour plot for Zn−O first shell coordination number versus Debye−Waller factor obtained from the EXAFS fit of the ~6.4 GPa aqueous solution. The innermost curve corresponds to the 95% confidence interval from which the statistical errors are determined.

3.2. Hydration Structure from MD Simulations. Molecular dynamics provides not only a reference structure for the EXAFS refinement but also can be used to access to a number of important (experimentally hidden) structural and dynamical observables. The Zn−O and Zn−H radial distribution functions and the corresponding running integration numbers calculated from the MD simulations at different pressure values are shown in Supporting Information, Figures 1S−5S. In all cases a well-defined first peak followed by a depletion zone can be observed, indicating the existence of a stable first hydration shell. In all simulations, the integration over Zn−O and Zn−H $g(r)$ first peaks gives coordination numbers of 6 and 12, respectively, in agreement with the EXAFS results. While the overall structure of the Zn^{2+} hydration complex is the same for all the investigated pressure

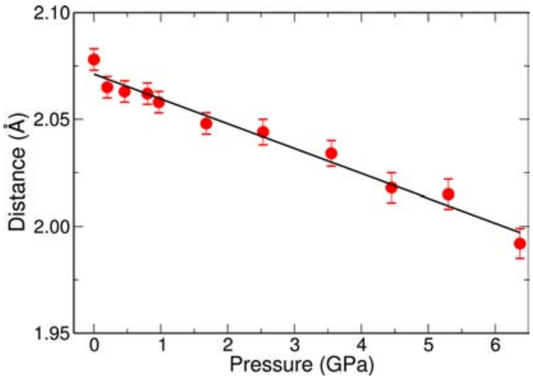

Figure 6. Zn−O first shell distances obtained from the EXAFS analysis versus pressure values.

values, a quite different dynamic behavior has emerged between the simulations carried out below 2.5 GPa and above this pressure value. In particular, no exchange events between first and second shell water molecules have been observed during the total simulation time in the trajectories carried out at ambient conditions, 1 and 2.5 GPa. This result is in agreement with the fact that the residence time of water molecules in the first hydration shell of Zn^{2+} at ambient conditions is in the microsecond time scale.[63] On the contrary, several exchange events between the first and the second coordination shells take place in the trajectories at 4.5 and 6.02 GPa. In particular, using a t^* value of 0.5 ps (see Methods section), 16 and 24 solvent exchange processes between the first hydration shell and the rest of the solvent have been observed in the simulations at 4.5 and 6.02 GPa, respectively. The results of our MD simulations show that at very high pressure the water exchange reaction of the Zn^{2+} ion follows an associative interchange mechanism with a heptahydrated intermediate. Heptacoordinated first shell clusters were detected in our trajectories only for very short periods of time (the longest lifetimes are 0.58 and 0.53 ps for the simulation at 4.5 and 6.02 GPa, respectively), meaning that the heptacoordinated clusters are reaction intermediates and not stable first shell complexes. The occurrence of exchange events following an associative interchange mechanism under high pressure can be explained by the very high compression and packing of the water molecules in the solution: a second

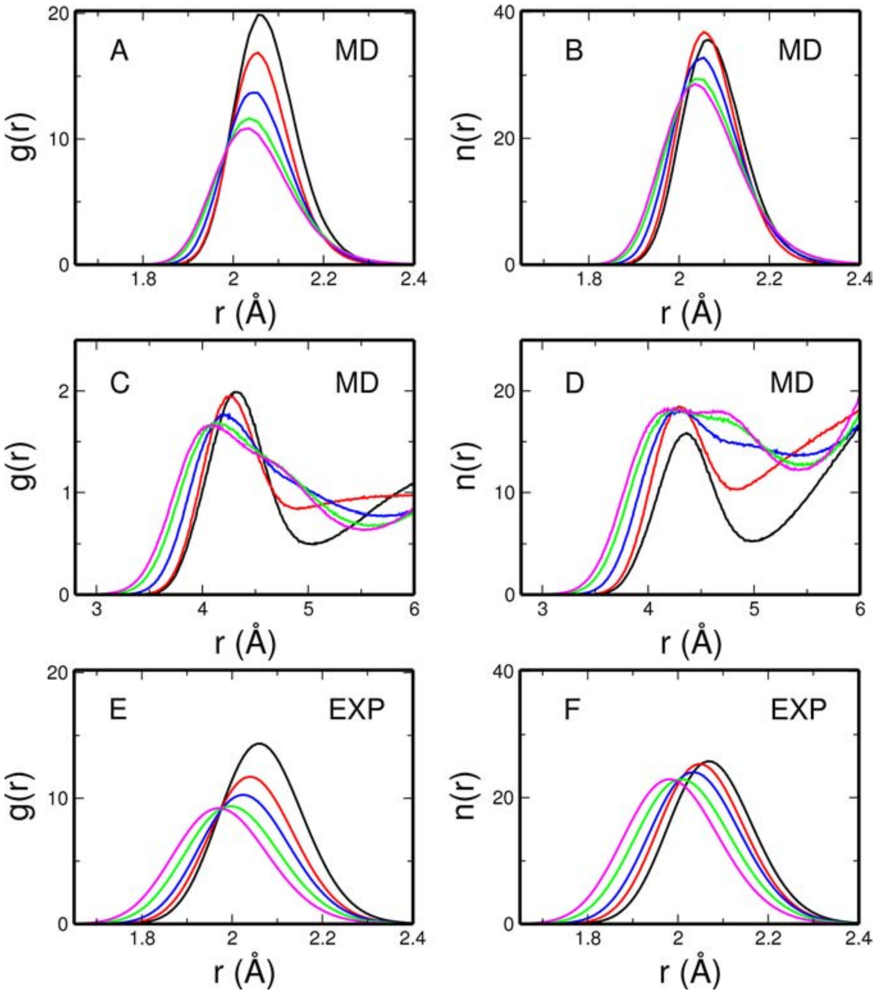

Figure 7. Panels A−D: Zn−O radial distribution functions $g(r)$ and radial densities $n(r) = 4\pi r^2 \rho g(r)$, obtained from the simulations carried out at 0.1 MPa (black line), 1.0 GPa (red line), 2.5 GPa (blue line), 4.5 (green line), and 6.02 GPa (magenta line). (A) Comparison of the Zn−O $g(r)$ first peak. (B) Comparison of the Zn−O $n(r)$ first peak. (C) Comparison of the Zn−O $g(r)$ second peak. (B) Comparison of the Zn−O $n(r)$ second peak. Panels E−F: Zn−O radial distribution functions $g(r)$ and radial densities $n(r)$obtained from the analysis of the EXAFS experimental data collected at 0.1 MPa (black line), 1.0 GPa (red line), 2.5 GPa (blue line), 4.5 (green line), and ∼6.4 GPa (magenta line). (E) Comparison of the Zn−O $g(r)$ first peak. (F) Comparison of the Zn−O $n(r)$ first peak.

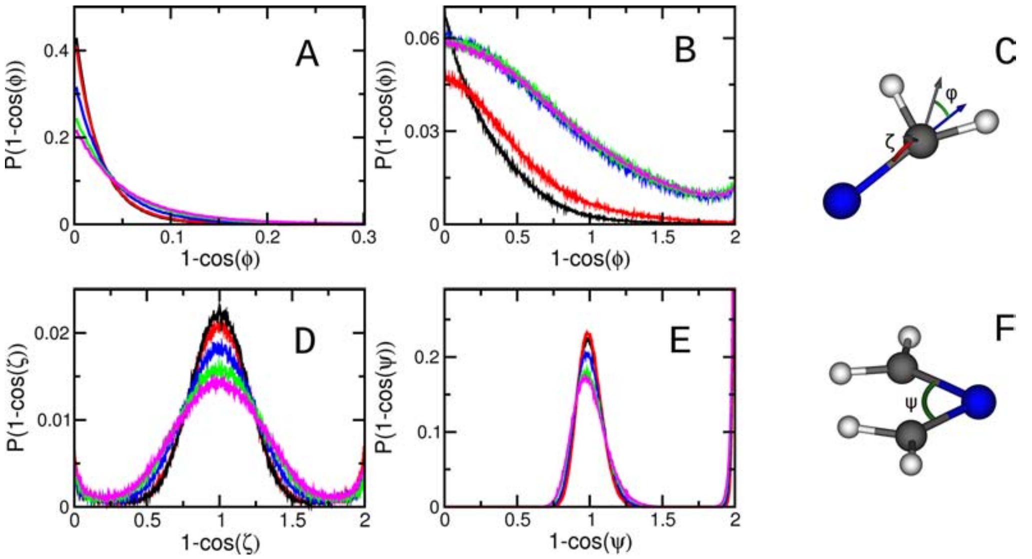

Figure 8. Angular distribution functions (a.d.f.) of the ϕ, ζ, and ψ angles obtained from the simulations carried out at 0.1 MPa (black line), 1.0 GPa (red line), 2.5 GPa (blue line), 4.5 GPa (green line), and 6.02 GPa (magenta line). (A) First hydration shell a.d.f of ϕ. (B) Second hydration shell a.d.f. of ϕ. (C) Definition of the ϕ and ζ angles. (D) First hydration shell a.d.f. of ζ. (E) First hydration shell a.d.f. of ψ. (F) Definition of the ψ angle.

shell water molecule is pushed into the Zn^{2+} first hydration shell, an unstable heptacoordinated complex is temporarily formed, and another water molecule then leaves the first coordination sphere with the re-establishment of the octahedral complex.

The comparison of the first peak of the Zn−O radial distribution functions is reported in panel A of Figure 7 for all the MD simulations. The radial distribution functions show a shortening of the peak position and a broadening of the first peak as pressure increases, a trend in agreement with the EXAFS results. To better visualize the pressure effects on the Zn−O radial distribution functions, we report in panel B of Figure 7 the corresponding radial densities $n(r) = 4\pi r^2 \rho g(r)$, where ρ is the density of oxygen atoms in the solutions. In such a case of strong ρ variations this quantity is better suited to appreciate the constancy of the first shell coordination number, that is, the integral of the first peak, and the actual peak broadening and shifts with pressure. The detailed comparison between EXAFS and MD results indicates that the simulation displays a smaller contraction of the first hydration shell with pressure and a smaller peak width. This comparison is quantified by modeling the MD Zn−O $n(r)$'s with gamma-like distributions (the same used for the EXAFS fit). The numerical results are summarized in Table 1, while the Zn−O $g(r)$ distributions obtained from the EXAFS data analysis are shown in panels E and F of Figure 7. The discrepancy between EXAFS and MD results indicates a limitation of the adopted physical model. In particular, the Zn−O interaction potential may reveal an excessive rigidity whose effect becomes more evident in high density solutions.[23] Still the analysis of the MD simulations provides a useful insight into the pressure trends of several structural and dynamical observables, experimentally not accessible, associated with important mechanisms related to ion hydration in aqueous solutions.

The effect of pressure changes is more evident on the structure of the second coordination shells, as shown in panels C and D of Figure 7. In this case the shift of the peak positions at shorter distances going from ambient conditions to 6.02 GPa is about 0.23 Å, larger than what observed for the first hydration shell (the second peak distances are 4.32 and 4.09 Å for the simulations at 0.1 MPa and 6.02 GPa, respectively). If the hydration number is always calculated by integration up to the Zn−O $g(r)$ second minimum, increasing coordination number values are obtained from the simulations (they are 10.9, 12.7, 30.0, 30.8, and 31.0 for the trajectories at 0.1 MPa, 1.0 GPa, 2.5 GPa, 4.5 GPa, and 6.02 GPa respectively). Moreover, the $g(r)$ changes qualitatively increasing the pressure in the zone after 4.5 Å, and for pressure values higher than 2.5 GPa the second hydration shell is not only shifted toward the metal ion but expands outward and is less separated from bulk water.

The a.d.f. obtained from the simulations of the ϕ, ζ, and ψ angles (plotted as functions of 1− cos (ϕ,ζ,ψ)) are depicted in Figure 8 together with the definition of the angles. Panel A of Figure 8 shows the a.d.f. of the ϕ angle for the water molecules belonging to the Zn^{2+} first hydration shell. The distribution functions calculated from the trajectories show very sharp peaks at $\cos(\phi) = 1$, as the oxygen atoms point toward the ion and wagging movements are very limited. The curves related to the simulation at 0.1 MPa and 1.0 GPa go to zero at about $\phi = 30°$ while the ϕ angle distribution becomes broader at higher pressure values, since at higher pressure there is an increase of rotational freedom of the first shell water molecules. Analysis of the second coordination shell a.d.f. gives quite different results: all of the simulations under high pressure show a change of slope and concavity as compared to the distribution obtained from the trajectory at 0.1 MPa, as the packing of the second hydration sphere forces the water molecules to deviate from the minimum potential energy alignment observed in the first simulation. Moreover, they are much broader, showing that in the compressed solutions wagging movements in the second hydration shell are much more important than at 0.1 MPa. Panel D of Figure 8 shows the a.d.f. of ζ angle. In all cases there is a well-defined peak centered at $\cos(\zeta) = 90°$, showing that the Zn−O vector is located most of the time in the water molecular plane, but the movements above and below the plane increase with increasing pressure. The a.d.f.'s for the ψ angle calculated at various pressures on first shell water molecules are shown in Panel E of Figure 8. All of the distribution functions have nearly coincident maxima at $1- \cos(\psi) = 1$ and $1- \cos(\psi) = 2$ (corresponding to ψ values of 90° and 180°), thus showing the existence of a stable octahedral coordination geometry, even at high pressures, in agreement with the EXAFS results. Moreover, the a.d.f.'s go to zero at intermediate values, since water molecules are strongly constrained in their positions and large distortions of the octahedral symmetry are not expected.

The three-dimensional structure of the Zn^{2+} first and second solvation shells can be observed looking at the spatial distribution functions calculated from the simulations at 0.1 MPa and 2.5 GPa, that are shown in Figure 9. The isodensity surfaces of oxygen and hydrogen atoms are colored green and red, respectively. The octahedral symmetry of the first hydration shell can be clearly seen both at 0.1 MPa and at 2.5 GPa, and the compression of the hydration shells going from ambient to the high-density conditions. The torus-shaped distribution of hydrogen atoms in the first hydration shell means that they are free to rotate around the water dipole. The outer green rings, which correspond to oxygen atoms in the second coordination shell, are much thicker and wider at 2.5 GPa, as more and more water molecules are packed into the second hydration shell, and the second coordination shell becomes more disordered and unstructured.

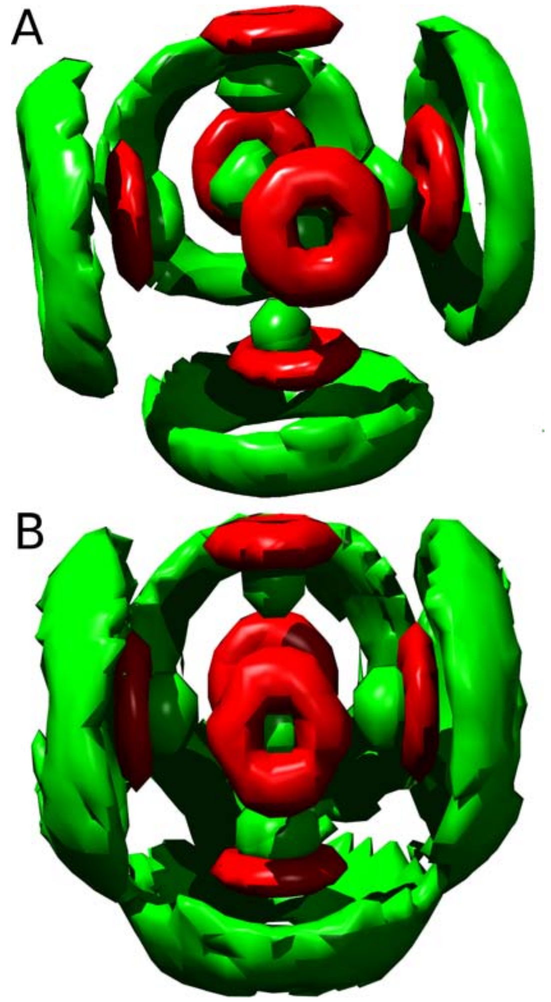

Figure 9. Spatial distribution functions of oxygen (green) and hydrogen (red) atoms obtained from the trajectory at 0.1 MPa (panel A) and 2.5 GPa (panel B). The isodensity surfaces at level 2.23 are shown.

3.3. Dynamical Properties from MD Simulations. As mentioned above, in the MD simulations carried out at pressure values lower than 2.5 GPa no solvent exchange processes between the first hydration shell and the rest of the solvent have been observed, while several exchange events between the first and second coordination shells have been detected for the trajectories at 4.5 and 6.02 GPa. For the latter two simulations, the rate of the water exchange processes has been evaluated by means of the residence time of the water molecules in the first hydration shell using the direct method (see Methods section). A t^* value of 0.5 ps has been employed as it corresponds to the average lifetime of a water−water hydrogen bond, and it has been found to be the more appropriate choice.[60] The mean residence times calculated from the simulations at 4.5 and 6.02 GPa are 3.75 and 2.50 ns, respectively. It is noteworthy to observe that while for systems with a very flexible first hydration shell, such as halide ions in aqueous solution, the calculated residence times have been shown to be strongly dependent on the choice of the t^* value, in the present case the results are less dependent on this parameter.[41] To give an idea, the same first shell residence time value has been obtained for the simulation at 6.02 GPa using a t^* value of either 0.5 or 2.0 ps. This is due to the high stability of the Zn^{2+} first shell complex for which the definition of the first hydration shell is less arbitrary and the exchange process much slower as compared, for example, to the Br^- ion in water.[41]

It is important to note that the method by Impey et al.[64] is one of the most used and reliable approaches to evaluate the residence time from MD simulations. Here, we did try to apply this procedure, but the obtained results were not reliable as the simulation lengths (10 ns) were not long enough to provide a statistically significant survival function for our systems, as the exchange events take place in the nanosecond time scale.

Even if the increase of pressure does not have a huge effect on the structure of the first hydration shell, it has a stronger effect on the dynamics of the water molecules surrounding the ion. This effect can be investigated by calculating the first rank reorientational correlation times of water molecules belonging to the Zn^{2+} first hydration shell and to bulk water. Figure 10 shows the trend of $C_1^{\alpha}(t)$ for the trajectories at 0.1 MPa, 2.5 GPa, and 6.02 GPa while all of the reorientational correlation times obtained from the three simulations are reported in Table 2. First of all, it is useful to compare the behavior of the different vectors within the same simulation, and in all cases the same general trend is observed. As far as the Zn^{2+} first hydration shell is concerned, the dominant motion is the rotation of $\mathbf{u}^N$ and $\mathbf{u}^{HH}$, that is, around the water dipole, as expected and as already observed for other divalent aqua ions.[65] This finding is in line with the results of the analysis of spatial distribution functions. The reorientational dynamics of the $\mathbf{u}^N$ vector is the fastest reorientation while the $\mathbf{u}^{HH}$ correlation time is slightly greater than that related to the $\mathbf{u}^N$ vector. In bulk water the $\mathbf{u}^N$ vector rotates faster than $\mathbf{u}^{HH}$ and $\mathbf{u}^D$, showing that water rotation in the bulk is anisotropic. This result has been already observed in MD simulations of pure water and it is possibly related to the geometry of the water model.[61] On the other hand, if we compare the results of the MD simulations, we clearly see that all of the correlations times, both in the first shell and in bulk water, decrease with increasing pressure. This means that water mobility increases, and it is a consequence of

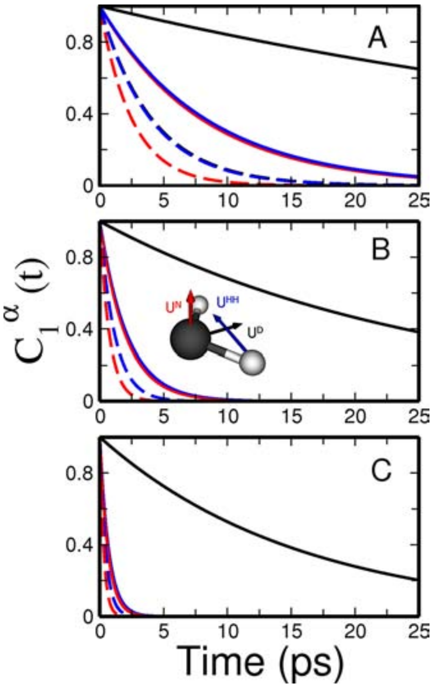

Figure 10. First rank reorientational correlation functions $C_1^{\alpha}(t)$ of water molecules belonging to the Zn^{2+} first hydration shell and to bulk water. Continuous lines refer to the ion first coordination shell, while dashed lines refer to bulk water. Different colors are related to the different vectors: $\mathbf{u}^D$ (black lines), $\mathbf{u}^{HH}$ (blue lines), and $\mathbf{u}^N$ (red lines). (A) Reorientational correlation functions obtained at 0.1 MPa. (B) Reorientational correlation functions obtained at 2.5 GPa. (C) Reorientational correlation functions obtained at 6.02 GPa.

the rupture of the hydrogen bond network caused by the pressure increase. Always as a consequence of the disruption of the hydrogen bond network the Zn^{2+} ion diffusion coefficient slightly increases (it is $0.7(0.1) \times 10^{-5}$ cm^2/s, $0.9(0.1) \times 10^{-5}$ cm^2/s, $1.0(0.3) \times 10^{-5}$ cm^2/s, $1.2(0.3) \times 10^{-5}$ cm^2/s, and $0.9(0.2) \times 10^{-5}$ cm^2/s for the simulations at 0.1 MPa, 1.0 GPa, 2.5 GPa, 4.5 GPa, and 6.02 GPa, respectively). Note that at ambient conditions we have obtained a diffusion coefficient in very good agreement with the experimental determination, which is equal to 0.703×10^{-5} cm^2/s.[66] We could not find any experimental values of this quantity at higher pressures.

4. CONCLUSIONS

In the present work we have investigated the Zn^{2+} hydration properties under high pressure conditions. Experimental advances of the high pressure large-volume setup at a Synchrotron Radiation Facility for X-ray absorption spectroscopy allowed us to access the Zn K-edge of an aqueous solution sample for the first time. The EXAFS analysis showed that the Zn^{2+} first shell hydration number does not vary with pressure, while the first hydration shell is contracted. Moreover, higher mobility of the water molecules in the first coordination sphere under high pressure has been highlighted by the trend of the Debye–Waller factors, that increase with pressure. Similarly, the results of the MD simulations of the Zn^{2+} ion in high-density water have shown that the octahedral structure of the Zn^{2+} first hydration shell remains stable also under high pressure, while the Zn–O first shell distance is shortened and the hydrated complex becomes more disordered. A very interesting picture of the dynamic behavior of the first hydration shell has emerged from the analysis of the simulations: up to 2.5 GPa no exchange events between first and second shell water molecules have been observed, while above this pressure value several exchange events take place in the solution following an associative interchange mechanism. This result can be explained by the very high compression and packing of the solvent which force second shell water molecules to enter the Zn^{2+} first hydration shell. The effect of the pressure changes is more evident on the structure of the second coordination shell which is compressed and becomes more disordered and unstructured with increasing pressure. Moreover, the increase of pressure has a strong effect on the dynamics of water, which has been investigated by calculating the reorientational correlation times of the water molecules surrounding the ion. The water mobility was found to increase, as a consequence of the rupture of the hydrogen bond network caused by the pressure increase. In line with these results, the Zn^{2+} diffusion coefficient was found to be slightly higher in the high density conditions.

This study of the Zn^{2+} ion in high-density water paves the route for future investigations on the hydration structure under high pressure conditions of other metal ions having more flexible hydration shells, such as Cd^{2+} and Hg^{2+}.

■ ASSOCIATED CONTENT

Ⓢ Supporting Information

Further details are given in Figures 1S–5S. This material is available free of charge via the Internet at http://pubs.acs.org.

■ AUTHOR INFORMATION

Corresponding Author

*E-mail: v.migliorati@caspur.it (V.M.), p.dangelo@caspur.it (P.D.).

Notes

The authors declare no competing financial interest.

Table 2. Reorientational Correlation Times (ps) of Water Molecules Belonging to the Zn^{2+} First Hydration Shell and to Bulk Water Obtained from the MD Simulations[a]

	vector	0.1 MPa	1.0 GPa	2.5 GPa	4.5 GPa	6.02 GPa
first shell	$\mathbf{u}^N$	7.7 (2)	5.0 (2)	1.97 (5)	0.90 (2)	0.71 (1)
	$\mathbf{u}^{HH}$	8.1 (2)	5.9 (2)	2.10 (5)	0.95 (2)	0.76 (1)
	$\mathbf{u}^D$	57 (4)	34 (2)	24 (1)	14.6 (6)	14.1 (8)
bulk water	$\mathbf{u}^N$	2.502 (3)	2.101 (3)	0.806 (1)	0.408 (1)	0.334 (1)
	$\mathbf{u}^{HH}$	3.903 (3)	3.310 (3)	1.211 (1)	0.605 (1)	0.489 (1)
	$\mathbf{u}^D$	3.901 (3)	3.309 (3)	1.236 (4)	0.648 (2)	0.529 (1)

[a] Standard deviations are given within parentheses.

■ ACKNOWLEDGMENTS

This work was supported by CASPUR with the Standard HPC Grant 2012 entitled: ”A combined X-ray absorption spectroscopy, Molecular Dynamics simulations and Quantum Mechanics calculation procedure for the structural characterization of ill-defined systems”. We acknowledge the European Synchrotron Radiation Facility for provision of synchrotron radiation facilities under the proposal HD-115, and we would like to thank all the staff of beamline BM29 for assistance in using the instrument. The authors gratefully acknowledge Prof. Mahendra Pal Verma of the Instituto de Investigaciones Electricas, Cuernavaca Morelos, Mexico, for having provided the density values of liquid water in the high pressure conditions.

■ REFERENCES

(1) Meade, C.; Jeanloz, R. *Science* **1991**, *252*, 68−72.

(2) Bina, C. R.; Navrotsky, A. *Nature (London)* **2000**, *408*, 844−847.

(3) Hogenboom, D. L.; J. S. Kargel, J. P. G.; Lee, L. *Icarus* **1995**, *115*, 258−277.

(4) Byrne, R. H.; Laurie, S. H. *Pure Appl. Chem.* **1999**, *71*, 871−890.

(5) Flanagin, L. W.; Balbuena, P. B.; Johnston, K. P.; Rossky, P. J. *J. Phys. Chem.* **1995**, *99*, 5196−5205.

(6) Sebastiani, D.; Parrinello, M. *ChemPhysChem* **2002**, *3*, 675−679.

(7) Yamaguchi, T. *J. Mol. Liq.* **1998**, *78*, 43−50.

(8) Bagchi, K.; Balasubramanian, S.; Klein, M. L. *J. Chem. Phys.* **1997**, *107*, 8561−8567.

(9) Kalinichev, A.; Gorbaty, Y.; Okhulkov, A. *J. Mol. Liq.* **1999**, *82*, 57−72.

(10) Soper, A. *Chem. Phys.* **2000**, *258*, 121−137.

(11) Soper, A. K.; Ricci, M. A. *Phys. Rev. Lett.* **2000**, *84*, 2881−2884.

(12) Schwegler, E.; Galli, G.; Gygi, F. *Phys. Rev. Lett.* **2000**, *84*, 2429−2432.

(13) Saitta, A. M.; Datchi, F. *Phys. Rev. E* **2003**, *67*, 020201.

(14) Strässle, T.; Saitta, A. M.; Godec, Y. L.; Hamel, G.; Klotz, S.; Loveday, J. S.; Nelmes, R. J. *Phys. Rev. Lett.* **2006**, *96*, 067801.

(15) English, N. J.; Tse, J. S. *Phys. Rev. Lett.* **2011**, *106*, 037801.

(16) Nilsson, A.; Pettersson, L. *Chem. Phys.* **2011**, *389*, 1−34.

(17) Filipponi, A.; De Panfilis, S.; Oliva, C.; Ricci, M. A.; D’Angelo, P.; Bowron, D. T. *Phys. Rev. Lett.* **2003**, *91*, 165505.

(18) Fedotova, M. V. *Russ. J. Phys. Chem. A* **2007**, *81*, 721−726.

(19) Klotz, S.; Bove, L. E.; Strassle, T.; Hansen, T. C.; Saitta, A. M. *Nat. Mater.* **2009**, *8*, 405−409.

(20) Ohtaki, H.; Radnai, T. *Chem. Rev.* **1993**, *93*, 1157−1204.

(21) D’Angelo, P.; Barone, V.; Chillemi, G.; Sanna, N.; Mayer-Klauke, W.; Pavel, N. V. *J. Am. Chem. Soc.* **2002**, *124*, 1958−1967.

(22) Inada, Y.; Hayashi, H.; Sugimoto, K.-i.; Funahashi, S. *J. Phys. Chem. A* **1999**, *103*, 1401−1406.

(23) Chillemi, G.; D’Angelo, P.; Pavel, N. V.; Sanna, N.; Barone, V. *J. Am. Chem. Soc.* **2002**, *124*, 1968−1976.

(24) Cauet, E.; Bogatko, S.; Weare, J. H.; Fulton, J. L.; Schenter, G. K.; Bylaska, E. J. *J. Chem. Phys.* **2010**, *132*, 194502.

(25) Wu, J. C.; Piquemal, J.-P.; Chaudret, R.; Reinhardt, P.; Ren, P. *J. Chem. Theory Comput.* **2010**, *6*, 2059−2070.

(26) Brancato, G.; Rega, N.; Barone, V. *Chem. Phys. Lett.* **2008**, *451*, 53−57.

(27) Mohammed, A.; Loeffler, H.; Inada, Y.; Tanada, K.; Funahashi, S. *J. Mol. Liq.* **2005**, *119*, 55−62.

(28) Arab, M.; Bougeard, D.; Smirnov, K. *Chem. Phys. Lett.* **2003**, *379*, 268−276.

(29) Fatmi, M. Q.; Hofer, T. S.; Randolf, B. R.; Rode, B. M. *J. Chem. Phys.* **2005**, *119*, 4514.

(30) Migliorati, V.; Chillemi, G.; Mancini, G.; Zitolo, A.; Tatoli, S.; Filipponi, A.; D’Angelo, P. *J. Phys.: Conf. Ser.* **2009**, *190*, 012057.

(31) Roccatano, D.; Berendsen, H. J. C.; D’Angelo, P. *J. Chem. Phys.* **1996**, *108*, 9487−9497.

(32) D’Angelo, P.; Pavel, N. V. *J. Chem. Phys.* **1999**, *111*, 5107−5115.

(33) Burattini, E.; D’Angelo, P.; Giglio, E.; Pavel, N. V. *J. Phys. Chem.* **1991**, *95*, 7880−7886.

(34) Chillemi, G.; Barone, V.; D’Angelo, P.; Mancini, G.; Persson, I.; Sanna, N. *J. Phys. Chem. B* **2005**, *109*, 9186−9193.

(35) D’Angelo, P.; Chillemi, G.; Barone, V.; Mancini, G.; Sanna, N.; Persson, I. *J. Phys. Chem. B* **2005**, *109*, 9178−9185.

(36) Spezia, R.; Duvail, M.; Vitorge, P.; Cartailler, T.; Tortajada, J.; D’Angelo, P.; Gaigeot, M.-P. *J. Phys. Chem. A* **2006**, *110*, 13081−13088.

(37) Chillemi, G.; Mancini, G.; Sanna, N.; Barone, V.; Della Longa, S.; Benfatto, M.; Pavel, N. V.; D’Angelo, P. *J. Am. Chem. Soc.* **2007**, *129*, 5430−5436.

(38) D’Angelo, P.; Migliorati, V.; Mancini, G.; Chillemi, G. *J. Phys. Chem. A* **2008**, *112*, 11833−11841.

(39) D’Angelo, P.; Migliorati, V.; Mancini, G.; Barone, V.; Chillemi, G. *J. Chem. Phys.* **2008**, *128*, 084502.

(40) D’Angelo, P.; Zitolo, A.; Migliorati, V.; Mancini, G.; Persson, I.; Chillemi, G. *Inorg. Chem.* **2009**, *48*, 10239−10248.

(41) D’Angelo, P.; Migliorati, V.; Guidoni, L. *Inorg. Chem.* **2010**, *49*, 4224−4231.

(42) Migliorati, V.; Mancini, G.; Chillemi, G.; Zitolo, A.; D’Angelo, P. *J. Phys. Chem. A* **2011**, *115*, 4798−4803.

(43) D’Angelo, P.; Zitolo, A.; Migliorati, V.; Chillemi, G.; Duvail, M.; Vitorge, P.; Abadie, S.; Spezia, R. *Inorg. Chem.* **2011**, *50*, 4572−4579.

(44) Migliorati, V.; Chillemi, G.; D’Angelo, P. *Inorg. Chem.* **2011**, *50*, 8509−8515.

(45) Migliorati, V.; Zitolo, A.; Chillemi, G.; D’Angelo, P. *ChemPlusChem* **2012**, *77*, 234−239.

(46) Filipponi, A.; Borowski, M.; Bowron, D. T.; Ansell, S.; Panfilis, S. D.; Di Cicco, A.; Itiè, J.-P. *Rev. Sci. Instrum.* **2000**, *71*, 2422−2432.

(47) Mathon, O.; Pascarelli, S. *AIP Conf. Proc.* **2004**, *705*, 498.

(48) Filipponi, A.; Borowski, M.; Loeffen, P. W.; De Panfilis, S.; Di Cicco, A.; Sperandini, F.; Minicucci, M.; Giorgetti, M. *J. Phys.: Condens. Matter* **1998**, *10*, 235−253.

(49) Filipponi, A.; De Panfilis, S.; Di Cicco, A. Temperature scanning techniques with tunable X-ray photons. In *X-ray Absorption Fine Structure - XAFS13*; Hedman, B., Pianetta, P., Eds.; American Institute of Physics: College Park, MD, 2007; Vol. *882*.

(50) Filipponi, A.; Di Cicco, A.; Natoli, C. R. *Phys. Rev. B* **1995**, *52*, 15122−15134.

(51) Filipponi, A.; Di Cicco, A. *Phys. Rev. B* **1995**, *52*, 15135−15149.

(52) Amovilli, C.; Barone, V.; Cammi, R.; Cances, E.; Cossi, M.; Mennucci, B.; Pomelli, C. S.; Tomasi, J. *Adv. Quantum Chem.* **1998**, *32*, 227−262.

(53) Berendsen, H. J. C.; Grigera, J. R.; Straatsma, T. P. *J. Phys. Chem.* **1987**, *91*, 6269−6271.

(54) Mark, P.; Nilsson, L. *J. Phys. Chem. A* **2001**, *105*, 9954−9960.

(55) Brodholt, J.; Wood, B. *J. Geophys. Res.* **1993**, *98*, 519−536.

(56) Verma, M. P. *Comput. Geosci.* **2003**, *29*, 1155−1163.

(57) Berendsen, H. J. C.; van der Spoel, D.; van Drunen, R. *Comput. Phys. Commun.* **1995**, *91*, 43−56.

(58) Essmann, U.; Perera, L.; Berkowitz, M. L.; Darden, T.; Lee, H.; Pedersen, L. G. *J. Chem. Phys.* **1995**, *103*, 8577−8593.

(59) Berendsen, H. J. C.; Postma, J. P. M.; van Gunsteren, W. F.; Di Nola, A.; Haak, J. R. *J. Chem. Phys.* **1984**, *81*, 3684−3690.

(60) Hofer, T. S.; Tran, H. T.; Schwenk, C. F.; Rode, B. M. *J. Comput. Chem.* **2004**, *25*, 211−217.

(61) van der Spoel, D.; van Maaren, P. J.; Berendsen, H. J. C. *J. Chem. Phys.* **1998**, *108*, 10220−10230.

(62) Madden, P.; Kivelson, D. A Consistent Molecular Treatment of Dielectric Phenomena. In *Advances in Chemical Physics*; John Wiley & Sons, Inc.: Hoboken, NJ, 2007.

(63) Eigen, M. *Pure Appl. Chem.* **1963**, *6*, 97−116.

(64) Impey, R. W.; Madden, P. A.; McDonald, I. R. *J. Chem. Phys.* **1983**, *87*, 5071−5083.

(65) Mancini, G.; Sanna, N.; Barone, V.; Migliorati, V.; D’Angelo, P.; Chillemi, G. *J. Phys. Chem. B* **2008**, *112*, 4694−4702.

(66) Lide, D. R. *CRC Handbook of Physics and Chemistry*, 85th ed.; CRC Press: Boca Raton, FL, 2005.